Self-Supervised Visual Representation Learning with Semantic Grouping

Xin Wen[1] **Bingchen Zhao**[2, 3] **Anlin Zheng**[1, 4] **Xiangyu Zhang**[4] **Xiaojuan Qi**[1]

[1]University of Hong Kong [2]University of Edinburgh [3]LunarAI [4]MEGVII Technology

{wenxin, xjqi}@eee.hku.hk zhaobc.gm@gmail.com
{zhenganlin, zhangxiangyu}@megvii.com

Abstract

In this paper, we tackle the problem of learning visual representations from unlabeled scene-centric data. Existing works have demonstrated the potential of utilizing the underlying complex structure within scene-centric data; still, they commonly rely on hand-crafted objectness priors or specialized pretext tasks to build a learning framework, which may harm generalizability. Instead, we propose contrastive learning from data-driven semantic slots, namely SlotCon, for joint semantic grouping and representation learning. The semantic grouping is performed by assigning pixels to a set of learnable prototypes, which can adapt to each sample by attentive pooling over the feature and form new slots. Based on the learned data-dependent slots, a contrastive objective is employed for representation learning, which enhances the discriminability of features, and conversely facilitates grouping semantically coherent pixels together. Compared with previous efforts, by simultaneously optimizing the two coupled objectives of semantic grouping and contrastive learning, our approach bypasses the disadvantages of hand-crafted priors and is able to learn object/group-level representations from scene-centric images. Experiments show our approach effectively decomposes complex scenes into semantic groups for feature learning and significantly benefits downstream tasks, including object detection, instance segmentation, and semantic segmentation. Code is available at `https://github.com/CVMI-Lab/SlotCon`.

1 Introduction

Existing self-supervised approaches have demonstrated that visual representations can be learned from unlabeled data by constructing pretexts such as transformation prediction [22], instance discrimination [72, 32], and masked image modeling [2, 31, 69], *etc*. Among them, approaches based on instance discrimination [29, 6, 7, 11], which treat each image as a single class and employ a contrastive learning objective for training, have attained remarkable success and are beneficial to boost performance on many downstream tasks.

However, this success is largely built upon the well-curated object-centric dataset ImageNet [15], which has a large gap with the real-world data for downstream applications, such as city scenes [13] or crowd scenes [48]. Directly applying the instance discrimination pretext to these real-world data by simply treating the scene as a whole overlooks its intrinsic structures (*e.g.*, multiple objects and complex layouts) and thus will limit the potential of pre-training with scene-centric data [63]. This leads to our focus: learning visual representations from unlabeled scene-centric data.

Recent efforts to address this problem can be coarsely categorized into two types of research. One stream extends the instance discrimination task to pixel level for dense representation learning [56,

36th Conference on Neural Information Processing Systems (NeurIPS 2022).

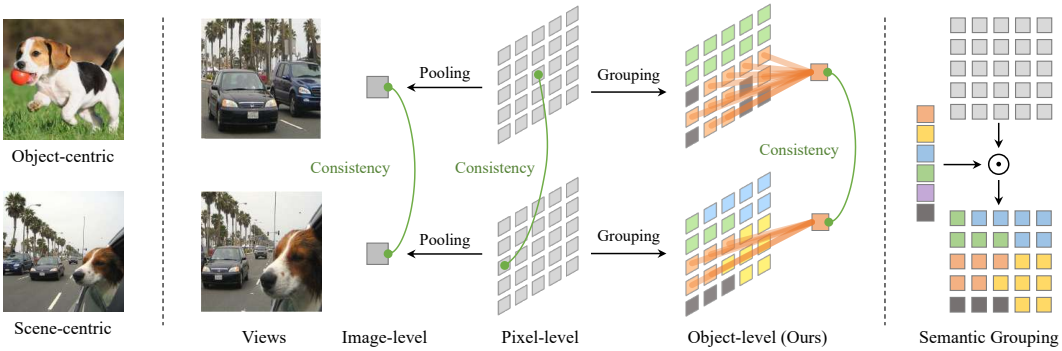

Figure 1: **Left:** Unlike object-centric images that highlight one iconic object, scene-centric images often contain multiple objects with complex layouts. This adds to the data diversity and increases the potential of image representations, yet it challenges previous learning paradigms that simply treat an image as a whole or individual pixels. **Middle:** Contrastive-learning objectives built upon different levels of image representations, in which object-level contrastive learning is viewed as the most suitable solution for scene-centric data. **Right:** We jointly learn a set of semantic prototypes in order to perform semantic grouping over the pixel-level representations and form object-centric slots.

68, 75], which shows strong performance in downstream dense prediction tasks. Yet, these methods still lack the ability to model object-level relationships presented in scene-centric data, which is crucial for learning representations. Although another stream of works attempts to perform object-level representation learning, most of them still heavily rely on domain-specific priors to discover objects, which include saliency estimators [64, 58], unsupervised object proposal algorithms [70, 74], hand-crafted segmentation algorithms [84, 35] or unsupervised clustering [36]. However, if the representation is supervised by hand-crafted objectness priors, it will be discouraged from learning objectness from the data itself and prone to mistakes from priors. Therefore, the capability and generalizability of the representation will be limited. In this work, we aim at a fully learnable and data-driven approach to enable learning representations from scene-centric data for enhanced effectiveness, transferability and generalizability.

We propose contrastive learning from data-driven semantic slots, namely SlotCon, for joint semantic grouping and representation learning. Semantic grouping is formulated as a feature-space pixel-level deep clustering problem where the cluster centers are initialized as a set of learnable semantic prototypes shared by the dataset, and grouping is achieved by assigning pixels to clusters. The cluster centers can then adapt to each sample by softly assigning pixels into cluster centers and aggregating their features via attentive pooling to form new ones, also called *slots*. Further, upon the learned slots from two random views of one image, a contrastive objective, which attempts to pull positive slots (*i.e.*, slots from the same prototype and sample) together and push away negative ones, is employed for representation learning. The optimized representations will enhance the discriminability of prototypes and slots, which conversely facilitates grouping semantically coherent pixels together. Compared with previous efforts, by simultaneously optimizing the two coupled objectives of semantic grouping and contrastive representation learning, our method bypasses the disadvantages of hand-crafted objectness priors[1] and is able to discover object/group-level representations from scene-centric images.

We extensively assess the representation learning ability of our model by conducting transfer learning evaluation on COCO [48] object detection, instance segmentation, and semantic segmentation on Cityscapes [13], PASCAL VOC [20], and ADE20K [86]. Our method shows strong results with both COCO pre-training and ImageNet-1K pre-training, bridging the gap between scene-centric and object-centric pre-training. As a byproduct, our method also achieves notable performance in unsupervised segmentation, showing strong ability in semantic concept discovery.

In summary, our main contributions in this paper are: 1) We show that the decomposition of natural scenes (semantic grouping) can be done in a learnable fashion and jointly optimized with the representations from scratch. 2) We demonstrate that semantic grouping can bring object-centric representation learning to large-scale real-world scenarios. 3) Combining semantic grouping and representation learning, we unleash the potential of scene-centric pre-training, largely close its gap with object-centric pre-training and achieve state-of-the-art results in various downstream tasks.

[1]Things can be different if the data is not reliable, see Section G in the appendix for details.

2 Related work

Our work is in the domain of self-supervised visual representation learning, where the goal is to learn visual representations without human annotations. We briefly review relevant works below.

Image-level self-supervised learning aims at learning visual representations by treating each image as one data sample. To this end, a series of pretext tasks are designed in which the labels are readily available without human annotations. Early explorations range from low-level pixel-wise reconstruction tasks that include denoising [66], inpainting [57], and cross-channel prediction [83] to higher-level instance discrimination [17], rotation prediction [22], context prediction [16], jigsaw puzzle [54], counting [55], and colorization [82]. Modern variants of instance discrimination [17] equipped with contrastive learning [62, 37] have shown strong potential in learning transferable visual representations [72, 8, 32, 60, 87, 85]. Other works differ in their learning objectives but still treat an image as a whole [29, 10, 81]. To further utilize the complex structure in natural images, some works exploit local crops [6, 73, 76, 63] while others either step to pixel- or object-level, detailed as follows.

Pixel-level contrastive learning extends the instance discrimination task from image-level feature vectors to feature maps [56, 49, 68, 75]. Their main differences lie in the way positive pixel-pairs are matched (spatial adjacency [56, 75], feature-space nearest-neighbor [68], sink-horn matching [49]), and the image-level baseline they build upon (MoCo v2 [56, 68], BYOL [49, 75]). Their pixel-level objective naturally helps learn dense representations that are favorable for dense prediction downstream tasks but lacks the grasp of holistic semantics and commonly require an auxiliary image-level loss to attain stronger performance [68, 75].

Object-level contrastive learning first discovers the objects in images and applies the contrastive objective over them, achieving a good balance in fine-grained structure and holistic semantics, yielding strong empirical gains with both object-centric [35, 36] and scene-centric data [74]. The key issue lies in finding objects in an image without supervision. Current works, however, still heavily rely on heuristic strategies that include saliency estimators [64, 58], selective-search [70, 74], hand-crafted segmentation algorithms [84, 35], or k-means clustering [36]. In contrast, our semantic grouping method is fully learnable and end to end, ensuring transferability and simplicity.

Unsupervised semantic segmentation is an emerging task that targets addressing semantic segmentation with only unlabeled images. The first attempt of IIC [41] maximizes the mutual information of augmented image patches, and later works [39, 64] rely on saliency estimators as a prior to bootstrap semantic pixel representations. Recently, PiCIE [40] adopt pixel-level deep clustering [5] to cluster the pixels into semantic groups, which SegDiscover [38] further improves by adopting super-pixels. On the other hand, Leopart [88], STEGO [30], and FreeSOLO [67] exploits pre-trained networks' attention maps for objectness. Still, they commonly rely on a (self-supervised) pre-trained network for initialization, while our method is trained fully from scratch.

Object-centric representation learning is viewed as an essential component of data-efficient, robust and interpretable machine learning algorithms [28]. Towards unsupervised object-centric representation learning, a series of works have been proposed [27, 3, 19, 50, 25, 24, 23]. Directly extracting objects from images is challenging due to the lack of supervision and thus prior works have long been restricted to synthetic data [43, 53, 1]. Recent works try to step toward real-world videos; however, they either adopt motion [77, 42] or depth [18] as a cue for objectness to solve this problem. Instead, our method shows that we can first explicitly optimize for desirable properties of clusters (that can describe an object) over the dataset, then retrieve the objects from an image with the learned prototypes. More importantly, it first shows the possibility of learning object-centric representations from large-scale unlabelled scene-centric natural images.

3 Method

3.1 Semantic grouping with pixel-level deep clustering

Given a dataset $\mathcal{D}$ of unlabeled images, we aim at learning a set of prototypes $\mathcal{S}$ that classifies each pixel into a meaningful group, such that pixels within the same group are semantic-consistent (have

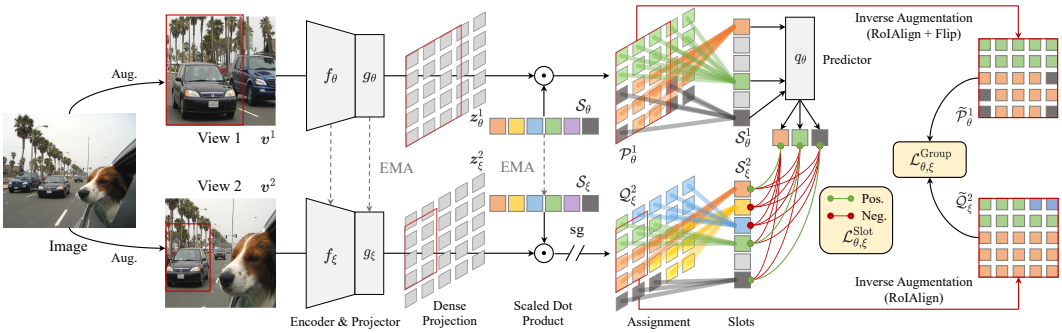

Figure 2: Overview of our proposed framework. Based on a shared pixel embedding function, the model learns to classify pixels into groups according to their feature similarity in a pixel-level deep clustering fashion (Sec. 3.1); the model produces group-level feature vectors (slots) through attentive pooling over the feature maps, and further performs group-level contrastive learning (Sec. 3.2). We omit the symmetrized loss computed by swapping the two views for simplicity. (*best viewed in color*)

similar feature representations), and pixels between different groups are semantic-incoherent. We find that this problem can be viewed as unsupervised semantic segmentation [22, 40], and solved with pixel-level deep clustering [5, 78, 6, 7].

Intuitively, a meaningful semantic grouping should be invariant to data augmentations. Thus, for different augmentations of the same image, we enforce the pixels that lie in the same location to have similar assignment scores w.r.t. the same set of cluster centers (prototypes). Besides consistent grouping, the groups should be different from each other to ensure that the learned representations are discriminative and avoid trivial solutions, *e.g.*, identical features. Together with standard techniques used in self-supervised learning (*e.g.*, non-linear projector and momentum teacher [29, 7], *etc.*), this leads to the following framework.

Specifically, as illustrated in Figure 2, our method contains two neural networks: the student network is parameterized by θ and include an encoder f_θ, a projector g_θ and a set of K learnable prototypes $\mathcal{S}_\theta = \left[\boldsymbol{s}_\theta^1, \boldsymbol{s}_\theta^2, \ldots, \boldsymbol{s}_\theta^K\right] \in \mathbb{R}^{K\times D}$; the teacher network holds the same architecture with the student, but uses a different set of weights ξ that updates as an exponential moving average of θ. Given an input image $\boldsymbol{x}$, two random augmentations are applied to produce two augmented views $\boldsymbol{v}^1$ and $\boldsymbol{v}^2$. Each augmented view $\boldsymbol{v}^l \in \{\boldsymbol{v}^1, \boldsymbol{v}^2\}$ is then encoded with an encoder f into a hidden feature map $\boldsymbol{h}^l \in \mathbb{R}^{H\times W\times D}$, and then transformed with a multilayer perceptron (MLP) g to get $\boldsymbol{z}^l = g\left(\boldsymbol{h}^l\right) \in \mathbb{R}^{H\times W\times D}$. We then compute the assignment $\mathcal{P}_\theta^l$ of the projections $\boldsymbol{z}_\theta^l$ with the corresponding prototypes $\mathcal{S}_\theta$, and enforce it to match the assignment $\mathcal{Q}_\xi^{l'}$ produced with another view $\boldsymbol{v}^{l'}$ by the teacher network. More precisely, with ℓ_2-normalized projections $\overline{\boldsymbol{z}} = \boldsymbol{z}/\|\boldsymbol{z}\|$ and prototypes $\overline{\boldsymbol{s}} = \boldsymbol{s}/\|\boldsymbol{s}\|$,

$$\mathcal{Q}_\xi^{l'} = \underset{K}{\operatorname{softmax}}\left(\left(\overline{\boldsymbol{z}}_\xi^{l'} \cdot \overline{\mathcal{S}}_\xi^\top - \boldsymbol{c}\right)/\tau_t\right), \quad \mathcal{P}_\theta^l = \underset{K}{\operatorname{softmax}}\left(\overline{\boldsymbol{z}}_\theta^l \cdot \overline{\mathcal{S}}_\theta^\top/\tau_s\right) \in \mathbb{R}^{H\times W\times K}, \tag{1}$$

with $\tau_s, \tau_t > 0$ temperature parameters that control the sharpness of the output distribution of the two networks. The $\boldsymbol{c}$ can be omitted and will be explained later. Note that the scale or layout of the two feature maps $\boldsymbol{z}_\theta^l$ and $\boldsymbol{z}_\xi^{l'}$ can be inconsistent due to geometric image augmentations, *e.g.*, random crop, scale or flip. So we perform the inverse augmentation process (including RoIAlign [33] and an optional flipping, details provided in Section A.1) on the predicted assignments to align their spatial locations: $\widetilde{\mathcal{Q}}_\xi^{l'} = \operatorname{invaug}\left(\mathcal{Q}_\xi^{l'}\right)$, $\widetilde{\mathcal{P}}_\theta^l = \operatorname{invaug}\left(\mathcal{P}_\theta^l\right)$. The inverse augmentation is performed on the assignments $\mathcal{Q}$ rather than the projections $\boldsymbol{z}$ to keep the context information out of the overlapping area for slot generation, which will be detailed in Section 3.2.

Based on the aligned assignments, we apply the cross-entropy loss $\mathcal{L}_{\theta,\xi}^{\text{CE}}\left(\boldsymbol{q}_\xi, \boldsymbol{p}_\theta\right) = -\sum_k \boldsymbol{q}_\xi^k \log \boldsymbol{p}_\theta^k$ to enforce the consistency in assignment score between spatial-aligned pixels from different views. The cross-entropy loss is averaged over all spatial locations to produce the grouping loss:

$$\mathcal{L}_{\theta,\xi}^{\text{Group}} = \frac{1}{H\times W}\sum_{i,j}\left[\mathcal{L}_{\theta,\xi}^{\text{CE}}\left(\widetilde{\mathcal{Q}}_\xi^2[i,j], \widetilde{\mathcal{P}}_\theta^1[i,j]\right) + \mathcal{L}_{\theta,\xi}^{\text{CE}}\left(\widetilde{\mathcal{Q}}_\xi^1[i,j], \widetilde{\mathcal{P}}_\theta^2[i,j]\right)\right]. \tag{2}$$

Directly optimizing the above objective resembles an unsupervised variant of Mean Teacher [59], which collapses as shown in [29]. In order to avoid collapsing, we follow [7] to maintain a *mean logit* $\boldsymbol{c} \in \mathbb{R}^K$ and reduce it when producing the teacher assignments $\mathcal{Q}_\xi$, as indicated in Eq. 1. The mean logit stores an exponential moving average of all the logits produced by the teacher network:

$$\boldsymbol{c} \leftarrow \lambda_c \boldsymbol{c} + (1-\lambda_c) \frac{1}{B \times H \times W} \sum_{i,j,k} \overline{\boldsymbol{z}}_\xi^{(i)}[j,k] \cdot \overline{\mathcal{S}}_\xi^\top \,, \tag{3}$$

where B stands for the batch size. Intuitively, reducing the mean logit amplifies the difference in assignment between different pixels, preventing all pixels from being assigned to the same prototype. Besides that, the teacher temperature τ_t is smaller than the student temperature τ_s to produce a sharper target and avoid uniform assignments. Both operations help avoid collapse and force the network to learn a meaningful semantic grouping.

Discussion with DINO. The resulting solution for semantic grouping may seem like a naive extension of DINO [7]. However, this is not the whole picture. DINO is an *image-level* representation learning approach that adopts a large number of prototypes (*e.g.*, 65536), while our objective is built on *pixel-level* representations and is tailored to learn meaningful semantic groups. Intuitively, DINO captures scene semantics that can be more complex and thus requires more prototypes to represent all scene-level variations, while our method learns object-level semantics which can be composed to depict a complicated scene and thus only requires a small number of prototypes (*e.g.*, 256 for COCO). Besides, the representation learning objective of DINO is built on prototypes that are *shared by the whole dataset*, while our method instead adapts prototypes for each image and performs contrastive learning over groups (detailed in Section 3.2). In summary, we present a novel view for the decoupling of pixel-level online clustering (*i.e.*, semantic grouping) and object-level representation learning.

3.2 Group-level representation learning by contrasting slots

Inspired by Slot Attention [50], we then reuse the assignments computed by the semantic grouping module in Eq. 1 to perform attentive pooling over the dense projections $\boldsymbol{z}$ to produce group-level feature vectors (rephrased as *slots*), as shown in Figure 2. Intuitively, as the $\mathrm{softmax}$ normalization applies to the slot dimension, the attention coefficients sum to one for each individual input feature vector. As a result, the soft assignments $\mathcal{A}$ of the dense projections $\boldsymbol{z}$ w.r.t. the corresponding prototypes $\mathcal{S}$ can also be viewed as the attention coefficients that describe how the prototypes decompose the dense projections into non-overlapping groups. This inspires us to decompose the dense projections with attentive pooling following [50]. Specifically, for a dense projection $\boldsymbol{z}_\theta^l$ produced from view $\boldsymbol{v}^l$, we extract K slots:

$$\mathcal{S}_\theta^l = \frac{1}{\sum_{i,j} \mathcal{A}_\theta^l[i,j]} \sum_{i,j} \mathcal{A}_\theta^l[i,j] \odot \boldsymbol{z}_\theta^l[i,j] \in \mathbb{R}^{K \times D}, \mathcal{A}_\theta^l = \underset{K}{\mathrm{softmax}} \left(\overline{\boldsymbol{z}}_\theta^l \cdot \overline{\mathcal{S}}_\theta^\top / \tau_t \right) \in \mathbb{R}^{H \times W \times K} \,, \tag{4}$$

where $\odot$ denotes the Hadamard product, and a similar operation applies for the teacher network to produce $\mathcal{S}_\xi^{l'}$. Since the initial slots are shared by the whole dataset, the corresponding semantic may be missing in a specific view $\boldsymbol{v}^l$, thus producing redundant slots. Therefore, we compute the following binary indicator $\mathbb{1}^l$ to mask out the slots that fail to occupy a dominating pixel:

$$\mathbb{1}_\theta^{k,l} = \exists_{i,j} \quad \text{such that} \quad \underset{K}{\mathrm{argmax}} \left(\mathcal{A}_\theta^l \right)[i,j] = k \,, \tag{5}$$

and $\mathbb{1}_\xi^{l'}$ is computed similarly. Following the literature in object-level SSL [64, 35, 74, 36], we then apply a contrastive learning objective to discriminate the slot that holds the same semantic across views from distracting slots with the InfoNCE [62] loss:

$$\mathcal{L}_{\theta,\xi}^{\text{InfoNCE}} \left(\mathcal{S}_\theta^l, \mathcal{S}_\xi^{l'} \right) = \frac{1}{K} \sum_{k=1}^{K} - \log \frac{\mathbb{1}_\theta^{k,l} \mathbb{1}_\xi^{k,l'} \exp \left(\overline{q_\theta} \left(\boldsymbol{s}_\theta^{k,l} \right) \cdot \overline{\boldsymbol{s}}_\xi^{k,l'} / \tau_c \right)}{\sum_{k'} \mathbb{1}_\theta^{k,l} \mathbb{1}_\xi^{k',l'} \exp \left(\overline{q_\theta} \left(\boldsymbol{s}_\theta^{k,l} \right) \cdot \overline{\boldsymbol{s}}_\xi^{k',l'} / \tau_c \right)} \,. \tag{6}$$

This objective helps maximize the similarity between different views of the same slot, while minimizing the similarity between slots from another view with different semantics and *all* slots from other

images. Note that here an additional predictor q_θ with the same architecture as the projector g_θ is applied to the slots $\mathcal{S}_\theta$ as empirically it yields stronger performance [11, 70, 36]. And the resulting slot-level contrastive loss also follows a symmetric design like Eq. 2:

$$\mathcal{L}_{\theta,\xi}^{\text{Slot}} = \mathcal{L}_{\theta,\xi}^{\text{InfoNCE}}\left(\mathcal{S}_\theta^1, \mathcal{S}_\xi^2\right) + \mathcal{L}_{\theta,\xi}^{\text{InfoNCE}}\left(\mathcal{S}_\theta^2, \mathcal{S}_\xi^1\right) . \tag{7}$$

3.3 The overall optimization objective

We jointly optimize the semantic grouping objective (Eq. 2) and the group-level contrastive learning objective (Eq. 7), controlled with a balancing factor λ_g:

$$\mathcal{L}_{\theta,\xi}^{\text{Overall}} = \lambda_g \mathcal{L}_{\theta,\xi}^{\text{Group}} + (1-\lambda_g)\mathcal{L}_{\theta,\xi}^{\text{Slot}} . \tag{8}$$

At each training step, the student network is optimized with gradients from the overall loss function: $\theta \leftarrow \text{optimizer}\left(\theta, \nabla_\theta \mathcal{L}_{\theta,\xi}^{\text{Overall}}, \eta\right)$, where η denotes the learning rate; and the teacher network updates as an exponential moving average of the student network: $\xi \leftarrow \lambda_t \xi + (1-\lambda_t)\theta$, with λ_t denoting the momentum value. After training, only the teacher encoder f_ξ is kept for downstream tasks.

4 Experiments

4.1 Implementation details

Pre-training datasets. We pre-train our models on COCO `train2017` [48] and ImageNet-1K [15], respectively. COCO `train2017` [48] contains $\sim$118K images of diverse scenes with objects of multiple scales, which is closer to real-world scenarios. In contrast, ImageNet-1K is a curated object-centric dataset containing more than $\sim$1.28M images, which is better for evaluating a model's potential with large-scale data. Besides, we also explore the limit of scene-centric pre-training on COCO+, *i.e.*, COCO `train2017` set plus the `unlabeled2017` set. See details in Table 1.

Table 1: Details of the datasets used for pre-training.

Dateset	#Img.	#Obj./Img.	#Class
ImageNet-1K [15]	1.28M	1.7	1000
COCO [48]	118K	7.3	80
COCO+ [48]	241K	N/A	N/A

Data augmentation. The image augmentation setting is the same as BYOL [29]: a 224×224-pixel random resized crop with a random horizontal flip, followed by a random color distortion, random grayscale conversion, random Gaussian blur, and solarization. The crop pairs without overlap are discarded during training.

Network architecture. We adopt ResNet-50 [34] as the default encoder for f_θ and f_ξ. The projector g_θ, g_ξ and predictor q_θ are MLPs whose architecture are identical to that in [7] with a hidden dimension of 4096 and an output dimension of 256.

Optimization. We adopt the LARS optimizer [79] to pre-train the model, with a batch size of 512 across eight NVIDIA 2080 Ti GPUs. Following [75], we utilize the cosine learning rate decay schedule [52] with a base learning rate of 1.0, linearly scaled with the batch size (LearningRate $=$ $1.0 \times$ BatchSize$/256$), a weight decay of 10^{-5}, and a warm-up period of 5 epochs. Following [74, 68, 75], the model is pre-trained for 800 epochs on COCO(+) and $100/200$ epochs on ImageNet, respectively. Following the common practice of [74, 75], the momentum value λ_t of the teacher model starts from 0.99 and is gradually increased to 1 following a cosine schedule. Synchronized batch normalization and automatic mixed precision are also enabled during training.

Hyper-parameters. The temperature values τ_s and τ_t in the student and teacher model are set to 0.1 and 0.07, respectively. Besides, the center momentum λ_c is set to 0.9. The default number of prototypes K is set to 256 for COCO(+) and 2048 for ImageNet, according to our empirical finding that setting the number of prototypes close to the number of human-annotated categories can help downstream performance. The temperature value τ_c for the contrastive loss is set to 0.2 following [11], and the default balancing ratio λ_g is set to 0.5.

4.2 Evaluation protocols

Following the common practice of previous self-supervised works [68, 75, 74], we evaluate the representation ability of the pre-trained model by taking it as the backbone of downstream tasks. Specifically, we add a newly initialized task-specific head to the pre-trained model for different downstream tasks, *i.e.*, object detection and instance segmentation on COCO [48], and semantic segmentation on PASCAL VOC [20], Cityscapes [13], and ADE20K [86].

Object detection and instance segmentation. We train a Mask R-CNN [33] model with R50-FPN [47] backbone implemented in `Detectron2` [71]. We fine-tune all layers end-to-end on COCO `train2017` split with the standard $1\times$ schedule and report AP, AP_{50}, AP_{75} on the `val2017` split. Following [68, 75, 74] we train with the standard $1\times$ schedule with SyncBN.

Semantic segmentation. The evaluation details of PASCAL VOC and Cityscapes strictly follow [32]. We take our network to initialize the backbone of a fully-convolutional network [51] and fine-tune all the layers end-to-end. For PASCAL VOC, we fine-tune the model on `train_aug2012` set for 30k iterations and report the mean intersection over union (mIoU) on the `val2012` set. For Cityscapes, we fine-tune on the `train_fine` set for 90k iterations and evaluate it on the `val_fine` set. For ADE20K, we follow the standard 80k iterations schedule of `MMSegmentation` [12].

Unsupervised semantic segmentation. We also evaluate the model's ability of discovering semantic groups in complex scenes, which is accomplished by performing unsupervised semantic segmentation on COCO-Stuff [4]. We follow the common practice in this field [41, 40, 38] to merge the labels into 27 categories (15 "stuff" categories and 12 "thing" categories), and evaluate with a subset created by [41]. We perform inference with resolution 320 and number of prototypes 27 following the standard practice. The predicted labels are matched with the ground truth through Hungarian matching [45], and evaluated on mIoU and pixel accuracy (pAcc).

4.3 Transfer learning results

COCO pre-training. In Table 2 we show the main results with COCO pre-training. There have been steady improvements in object-level pre-training with COCO, in which the top performance methods are DetCon [46] and ORL [74], which still rely on objectness priors like selective-search [61] or hand-crafted segmentation algorithms [21], yet they still fail to beat the pixel-level state-of-the-

Table 2: **Main transfer results with COCO pre-training.** We report the results in COCO [48] object detection, COCO instance segmentation, and semantic segmentation in Cityscapes [13], PASCAL VOC [20] and ADE20K [86]. Compared with other image-, pixel-, and object-level self-supervised learning methods, our method shows consistent improvements over different tasks without leveraging multi-crop [6] and objectness priors. (†: re-impl. w/ official weights; ‡: full re-impl.)

Method	Epochs	Multi crop	Obj. Prior	COCO detection			COCO segmentation			Semantic seg. (mIoU)		
				AP^{b}	$\text{AP}^{\text{b}}_{50}$	$\text{AP}^{\text{b}}_{75}$	AP^{m}	$\text{AP}^{\text{m}}_{50}$	$\text{AP}^{\text{m}}_{75}$	City.	VOC	ADE
random init.	-	✗	✗	32.8	50.9	35.3	29.9	47.9	32.0	65.3	39.5	29.4
Image-level approaches												
MoCo v2‡ [9]	800	✗	✗	38.5	58.1	42.1	34.8	55.3	37.3	73.8	69.2	36.2
Revisit.† [63]	800	✓	✗	40.1	60.2	43.6	36.3	57.3	38.9	75.3	70.6	37.0
Pixel-level approaches												
Self-EMD [49]	800	✗	✗	39.3	60.1	42.8	-	-	-	-	-	-
DenseCL† [68]	800	✗	✗	39.6	59.3	43.3	35.7	56.5	38.4	75.8	71.6	37.1
PixPro‡ [75]	800	✗	✗	40.5	60.5	44.0	36.6	57.8	39.0	75.2	**72.0**	38.3
Object / Group-level approaches												
DetCon† [35]	1000	✗	✓	39.8	59.5	43.5	35.9	56.4	38.7	76.1	70.2	38.1
ORL† [74]	800	✓	✓	40.3	60.2	44.4	36.3	57.3	38.9	75.6	70.9	36.7
Ours (SlotCon)	800	✗	✗	**41.0**	**61.1**	**45.0**	**37.0**	**58.3**	**39.8**	**76.2**	71.6	**39.0**

art PixPro [75].[2] Our method alleviates such limitations and significantly improves over current object-level methods in all tasks, achieving consistent improvement over the previous approaches and even several methods that were pre-trained on the larger dataset ImageNet-1K (Table 4). It is also notable that our method can achieve a better performance on the most large and challenging dataset for segmentation, ADE20K, adding to the significance of this work.

COCO+ pre-training. In Table 3, we report the results with COCO+ pre-training. The COCO+ is COCO `train2017` plus `unlabeled2017` set, which roughly doubles the number of training images and greatly adds to the data diversity. Our method further sees a notable gain in all tasks with extended COCO+ data, and even shows comparable results with our best-performing model pre-trained on ImageNet-1K ($5\times$ large of COCO+), showing the great potential of scene-centric pre-training.

Table 3: **Pushing the limit of scene-centric pre-training.** Our method further sees a notable gain in all tasks with extended COCO+ data, showing the great potential of scene-centric pre-training.

Method	Dataset	Epochs	COCO detection			COCO segmentation			Semantic seg. (mIoU)		
			AP^b	AP^b_{50}	AP^b_{75}	AP^m	AP^m_{50}	AP^m_{75}	City.	VOC	ADE
SlotCon	COCO	800	41.0	61.1	45.0	37.0	58.3	39.8	76.2	71.6	39.0
SlotCon	ImageNet	100	41.4	61.6	45.6	37.2	58.5	39.9	75.4	73.1	38.6
SlotCon	ImageNet	200	**41.8**	**62.2**	45.7	**37.8**	59.1	**40.7**	76.3	**75.0**	38.8
ORL [74]	COCO+	800	40.6	60.8	44.5	36.7	57.9	39.3	-	-	-
SlotCon	COCO+	800	**41.8**	**62.2**	**45.8**	**37.8**	**59.4**	40.6	**76.5**	73.9	**39.2**

ImageNet-1K pre-training. In Table 4, we also benchmark our method with ImageNet-1K pre-training and show its compatibility with object-centric data. Without selective-search for object proposals and without pre-training and transferring the FPN head, our method still beats most of the current works and largely closes the gap with the detection-specialized method SoCo.

Table 4: **Main transfer results with ImageNet-1K pre-training.** Our method is also compatible with object-centric data and shows consistent improvements over different tasks without using FPN [47] and objectness priors. (†: re-impl. w/ official weights; ‡: full re-impl.)

Method	Epochs	w/ FPN	Obj. Prior	COCO detection			COCO segmentation			Semantic seg. (mIoU)		
				AP^b	AP^b_{50}	AP^b_{75}	AP^m	AP^m_{50}	AP^m_{75}	City.	VOC	ADE
random init.	-	✗	✗	32.8	50.9	35.3	29.9	47.9	32.0	65.3	39.5	29.4
supervised	100	✗	✗	39.7	59.5	43.3	35.9	56.6	38.6	74.6	74.4	37.9
Image-level approaches												
MoCo v2† [9]	800	✗	✗	40.4	60.1	44.2	36.5	57.2	39.2	76.2	73.7	36.9
DetCo† [73]	200	✗	✗	40.1	61.0	43.9	36.4	58.0	38.9	76.0	72.6	37.8
InsLoc† [76]	200	✓	✗	40.9	60.9	44.7	36.8	57.8	39.4	75.4	72.9	37.3
Pixel-level approaches												
DenseCL† [68]	200	✗	✗	40.3	59.9	44.3	36.4	57.0	39.2	76.2	72.8	38.1
PixPro† [75]	100	✗	✗	40.7	60.5	44.8	36.8	57.4	39.7	**76.8**	73.9	38.2
Object / Group-level approaches												
DetCon [35]	200	✗	✓	40.6	-	-	36.4	-	-	75.5	72.6	-
SoCo‡ [70]	100	✓	✓	41.6	61.9	45.6	37.4	58.8	40.2	76.5	71.9	37.8
Ours (SlotCon)	100	✗	✗	41.4	61.6	45.6	37.2	58.5	39.9	75.4	73.1	38.6
Ours (SlotCon)	200	✗	✗	**41.8**	**62.2**	**45.7**	**37.8**	**59.1**	**40.7**	76.3	**75.0**	**38.8**

4.4 Unsupervised semantic segmentation results

Given our approach's consistent improvement in representation learning, we further analysis of how well our semantic grouping component can parse scenes quantitatively and qualitatively. It should be

[2] PixPro aggregates the global context with self-attention [65], so each pixel can also be viewed as an object-level embedding.

Table 5: Main results in COCO-Stuff unsupervised semantic segmentation.

Method	mIoU	pAcc
MaskContrast [64]	8.86	23.03
PiCIE + H. [40]	14.36	49.99
SegDiscover [38]	14.34	**56.53**
Ours (SlotCon)	**18.26**	42.36

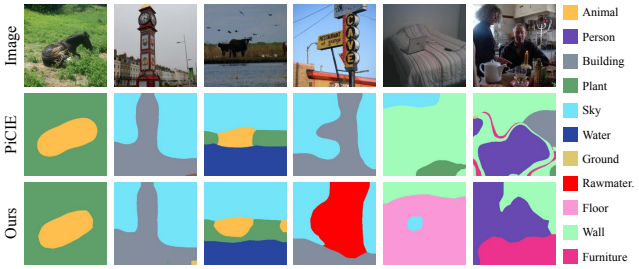

clarified that this is just to help understand the learned prototypes, and not to propose a new SOTA. Unlike current SSL approaches that exhaustively enumerate the massive object proposals and report the best score [7, 36], we follow the common practice of unsupervised semantic segmentation [41, 40] to match the predicted results with the ground-truth using the Hungarian algorithm [45], where each ground-truth label is assigned to a prototype mutual-exclusively. For fair comparisons, the model used for evaluation is trained with $K = 27$ to match the number of categories of COCO-Stuff. As shown in Table 5, our method can surpass the previous works PiCIE [40] and SegDiscover [38] with 4 points higher mIoU. Meanwhile, the pAcc is lower since we train the model with a lower resolution (7×7 v.s. 80×80 feature map). Besides Table 5, we also depict the visualization results, in which our method distinguishes confusing objects apart (4th column) and successfully localizes small objects (5th column). Since we only need to separate pixels with different semantics within the same image, the errors in category prediction can be ignored.

4.5 Ablation study

Table 6: **Ablation studies with COCO 800 epochs pre-training.** We show the AP^b on COCO objection detection and mIoU on Cityscapes, PASCAL VOC, and ADE20K semantic segmentation. The default options are marked with a gray background.

(a) **Number of prototypes**

K	COCO	City	VOC	ADE
128	40.7	**76.4**	**71.9**	38.5
256	**41.0**	76.2	71.6	39.0
512	40.9	75.6	71.6	38.9
1024	40.7	75.8	70.9	**39.1**

(b) **Loss balancing**

λ_g	COCO	City	VOC	ADE
0.3	**41.0**	76.1	**72.1**	37.9
0.5	**41.0**	**76.2**	71.6	**39.0**
0.7	40.5	75.2	71.5	38.4
1.0	40.4	74.2	70.1	38.6

(c) **Teacher temperature**

τ_t	COCO	City	VOC	ADE
0.04	40.4	75.5	70.2	37.9
0.07	**41.0**	**76.2**	**71.6**	**39.0**

Number of prototypes K. Table 6a ablates the number of prototypes, we observe that the most suitable K for COCO detection is 256, which is close to its real semantic class number 172 (thing + stuff) [4]. Besides, the performance on Cityscapes and PASCAL VOC have a consistent tendency to drop, while the performance on ADE20K is consistently good if K is big enough. We hypothesize that a suitable K can encourage learning data-specific semantic features, which are only helpful when the pre-training and downstream data are alike (from COCO to COCO); increasing K produces fine-grained features that may lack discriminability in semantics but hold better transferability to ADE20K that require fine-grained segmentation [14].

Loss balancing weight λ_g. Table 6b ablates the balancing between the semantic grouping loss and the group-level contrastive loss, where the best balance is achieved with both losses treated equally. It is notable that when $\lambda_g = 1.0$, only the semantic grouping loss is applied, and the performance drops considerably, indicating the importance of our group-level contrastive loss for learning good representations.

Teacher temperature τ_t. Table 6c ablates the teacher model's temperature parameter, indicating that a softer teacher distribution with $\tau_t = 0.07$ helps achieve better performance.

4.6 Probing the prototypes

Finally, we analyze whether the prototypes learn semantic meanings by visualizing their nearest neighbors in COCO `val2017` split. We first perform semantic grouping on each image to split them into non-overlapping groups (segments), then pool each group to a feature vector, and retrieve the

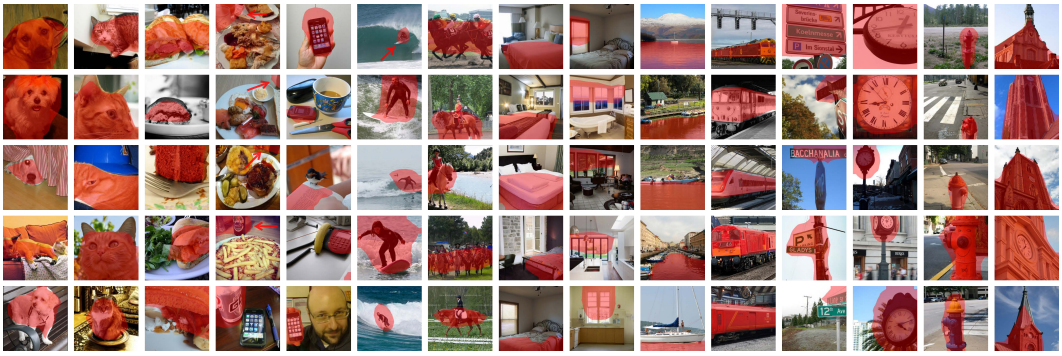

Figure 3: **Examples of visual concepts discovered by SlotCon from the COCO** `val2017` **split.** Each column shows the top 5 segments retrieved with the same prototype, marked with reddish masks or arrows. Our method can discover visual concepts across various scenarios and semantic granularities regardless of small object size and occlusion. (*best viewed in color*)

top 5 nearest-neighbor segments for each prototype according to cosine similarity. As shown in Figure 3, the prototypes well bind to semantic meanings that cover a wide range of scenarios and semantic granularities from animals, foods, and sports, to furniture, buildings, etc., localizing them well regardless of small object size and occlusion; and notably, *without any human annotation*.

5 Discussion on the emergence of objectness

It should be clarified that the discovered objectiveness is at the semantic level, and object instances with identical semantics can be indistinguishable. Concerning the emergence of objectness, we impose geometric-covariance and photometric-invariance as guiding cues which force the model to decompose a large complex dataset into a small number of clusters through optimizing feature space and cluster centers. The emergence of objects/parts that are compositional and thus occupy a reasonable number of prototypes, can be viewed as a natural consequence under such conditions. Concerning granularity, our intuition is that the prototype number and the dataset distribution generate a bottleneck for the granularity of groups. For example, in the COCO dataset, with 256 prototypes, the model finds that splitting animals into cats, dots, elephants, *etc*., is enough and won't further separate them. In contrast, for humans (the most occupying category of COCO), as shown in the appendix, the model discovers not only human parts (Figure 10) but also different types of activities (Figure 11), indicating that parts are more helpful in this scenario and deserve more prototypes.

6 Conclusion

This work presents a unified framework for joint semantic grouping and representation learning from unlabeled scene-centric images. The semantic grouping is performed by assigning pixels to a set of learnable prototypes, which can adapt to each sample by attentive pooling over the feature map and form new slots. Based on the learned data-dependent slots, a contrastive objective is employed for representation learning, enhancing features' discriminability and facilitating the grouping of semantically coherent pixels together. By simultaneously optimizing the two coupled objectives of semantic grouping and contrastive learning, the proposed approach bypasses the disadvantages of handcrafted priors and can learn object/group-level representations from scene-centric images. Experiments show the proposed approach effectively decomposes complex scenes into semantic groups for feature learning and significantly facilitates downstream tasks, including object detection, instance segmentation, and semantic segmentation.

Acknowledgments

This work has been supported by Hong Kong Research Grant Council - Early Career Scheme (Grant No. 27209621), HKU Startup Fund, and HKU Seed Fund for Basic Research. The authors acknowledge SmartMore, LunarAI, and MEGVII for partial computing support.

References

[1] Federico Baldassarre and Hossein Azizpour. Towards Self-Supervised Learning of Global and Object-Centric Representations. *arXiv:2203.05997 [cs]*, March 2022.

[2] Hangbo Bao, Li Dong, and Furu Wei. BEiT: BERT Pre-Training of Image Transformers. *arXiv:2106.08254 [cs]*, June 2021.

[3] Christopher P. Burgess, Loic Matthey, Nicholas Watters, Rishabh Kabra, Irina Higgins, Matt Botvinick, and Alexander Lerchner. MONet: Unsupervised Scene Decomposition and Representation. *arXiv:1901.11390 [cs, stat]*, January 2019.

[4] Holger Caesar, Jasper Uijlings, and Vittorio Ferrari. COCO-Stuff: Thing and Stuff Classes in Context. In *2018 IEEE/CVF Conference on Computer Vision and Pattern Recognition*, pages 1209–1218, June 2018.

[5] Mathilde Caron, Piotr Bojanowski, Armand Joulin, and Matthijs Douze. Deep Clustering for Unsupervised Learning of Visual Features. In Vittorio Ferrari, Martial Hebert, Cristian Sminchisescu, and Yair Weiss, editors, *Computer Vision – ECCV 2018*, pages 139–156, Cham, 2018. Springer International Publishing.

[6] Mathilde Caron, Ishan Misra, Julien Mairal, Priya Goyal, Piotr Bojanowski, and Armand Joulin. Unsupervised learning of visual features by contrasting cluster assignments. In H. Larochelle, M. Ranzato, R. Hadsell, M. F. Balcan, and H. Lin, editors, *Advances in Neural Information Processing Systems*, volume 33, pages 9912–9924. Curran Associates, Inc., 2020.

[7] Mathilde Caron, Hugo Touvron, Ishan Misra, Hervé Jégou, Julien Mairal, Piotr Bojanowski, and Armand Joulin. Emerging Properties in Self-Supervised Vision Transformers. In *Proceedings of the IEEE/CVF International Conference on Computer Vision*, pages 9650–9660, 2021.

[8] Ting Chen, Simon Kornblith, Mohammad Norouzi, and Geoffrey Hinton. A Simple Framework for Contrastive Learning of Visual Representations. In *Proceedings of the 37th International Conference on Machine Learning*, pages 1597–1607. PMLR, November 2020.

[9] Xinlei Chen, Haoqi Fan, Ross Girshick, and Kaiming He. Improved Baselines with Momentum Contrastive Learning. *arXiv:2003.04297 [cs]*, March 2020.

[10] Xinlei Chen and Kaiming He. Exploring Simple Siamese Representation Learning. In *2021 IEEE/CVF Conference on Computer Vision and Pattern Recognition (CVPR)*, pages 15745–15753, Nashville, TN, USA, June 2021. IEEE.

[11] Xinlei Chen, Saining Xie, and Kaiming He. An Empirical Study of Training Self-Supervised Vision Transformers. In *Proceedings of the IEEE/CVF International Conference on Computer Vision*, pages 9640–9649, 2021.

[12] MMSegmentation Contributors. MMSegmentation: Openmmlab semantic segmentation toolbox and benchmark. `https://github.com/open-mmlab/mmsegmentation`, 2020.

[13] Marius Cordts, Mohamed Omran, Sebastian Ramos, Timo Rehfeld, Markus Enzweiler, Rodrigo Benenson, Uwe Franke, Stefan Roth, and Bernt Schiele. The Cityscapes Dataset for Semantic Urban Scene Understanding. In *2016 IEEE Conference on Computer Vision and Pattern Recognition (CVPR)*, pages 3213–3223. IEEE Computer Society, June 2016.

[14] Quan Cui, Bingchen Zhao, Zhao-Min Chen, Borui Zhao, Renjie Song, Jiajun Liang, Boyan Zhou, and Osamu Yoshie. Discriminability-Transferability Trade-Off: An Information-Theoretic Perspective. *arXiv:2203.03871 [cs]*, March 2022.

[15] Jia Deng, Wei Dong, Richard Socher, Li-Jia Li, Kai Li, and Li Fei-Fei. ImageNet: A large-scale hierarchical image database. In *2009 IEEE Conference on Computer Vision and Pattern Recognition*, pages 248–255, June 2009.

[16] Carl Doersch, Abhinav Gupta, and Alexei A. Efros. Unsupervised Visual Representation Learning by Context Prediction. In *2015 IEEE International Conference on Computer Vision (ICCV)*, pages 1422–1430, December 2015.

[17] Alexey Dosovitskiy, Philipp Fischer, Jost Tobias Springenberg, Martin Riedmiller, and Thomas Brox. Discriminative unsupervised feature learning with exemplar convolutional neural networks. *IEEE Transactions on Pattern Analysis and Machine Intelligence*, 38(9):1734–1747, 2015.

[18] Gamaleldin F Elsayed, Aravindh Mahendran, Sjoerd van Steenkiste, Klaus Greff, Michael C Mozer, and Thomas Kipf. Savi++: Towards end-to-end object-centric learning from real-world videos. *arXiv preprint arXiv:2206.07764*, 2022.

[19] Martin Engelcke, Adam R. Kosiorek, Oiwi Parker Jones, and Ingmar Posner. GENESIS: Generative Scene Inference and Sampling with Object-Centric Latent Representations. In *International Conference on Learning Representations*, September 2019.

[20] Mark Everingham, S. M. Ali Eslami, Luc Van Gool, Christopher K. I. Williams, John Winn, and Andrew Zisserman. The Pascal Visual Object Classes Challenge: A Retrospective. *International Journal of Computer Vision*, 111(1):98–136, January 2015.

[21] Pedro F. Felzenszwalb and Daniel P. Huttenlocher. Efficient Graph-Based Image Segmentation. *International Journal of Computer Vision*, 59(2):167–181, September 2004.

[22] Spyros Gidaris, Praveer Singh, and Nikos Komodakis. Unsupervised Representation Learning by Predicting Image Rotations. In *International Conference on Learning Representations*, February 2018.

[23] Anirudh Goyal, Aniket Rajiv Didolkar, Nan Rosemary Ke, Charles Blundell, Philippe Beaudoin, Nicolas Heess, Michael Curtis Mozer, and Yoshua Bengio. Neural production systems. In A. Beygelzimer, Y. Dauphin, P. Liang, and J. Wortman Vaughan, editors, *Advances in Neural Information Processing Systems*, 2021.

[24] Anirudh Goyal, Alex Lamb, Phanideep Gampa, Philippe Beaudoin, Charles Blundell, Sergey Levine, Yoshua Bengio, and Michael Curtis Mozer. Factorizing declarative and procedural knowledge in structured, dynamical environments. In *International Conference on Learning Representations*, 2021.

[25] Anirudh Goyal, Alex Lamb, Jordan Hoffmann, Shagun Sodhani, Sergey Levine, Yoshua Bengio, and Bernhard Schölkopf. Recurrent independent mechanisms. In *International Conference on Learning Representations*, 2021.

[26] Priya Goyal, Piotr Dollár, Ross Girshick, Pieter Noordhuis, Lukasz Wesolowski, Aapo Kyrola, Andrew Tulloch, Yangqing Jia, and Kaiming He. Accurate, Large Minibatch SGD: Training ImageNet in 1 Hour, April 2018.

[27] Klaus Greff, Raphaël Lopez Kaufman, Rishabh Kabra, Nick Watters, Christopher Burgess, Daniel Zoran, Loic Matthey, Matthew Botvinick, and Alexander Lerchner. Multi-Object Representation Learning with Iterative Variational Inference. In *Proceedings of the 36th International Conference on Machine Learning*, pages 2424–2433. PMLR, May 2019.

[28] Klaus Greff, Sjoerd van Steenkiste, and Jürgen Schmidhuber. On the Binding Problem in Artificial Neural Networks. *arXiv:2012.05208 [cs]*, December 2020.

[29] Jean-Bastien Grill, Florian Strub, Florent Altché, Corentin Tallec, Pierre Richemond, Elena Buchatskaya, Carl Doersch, Bernardo Avila Pires, Zhaohan Guo, Mohammad Gheshlaghi Azar, Bilal Piot, koray kavukcuoglu, Remi Munos, and Michal Valko. Bootstrap your own latent - a new approach to self-supervised learning. In H. Larochelle, M. Ranzato, R. Hadsell, M. F. Balcan, and H. Lin, editors, *Advances in Neural Information Processing Systems*, volume 33, pages 21271–21284. Curran Associates, Inc., 2020.

[30] Mark Hamilton, Zhoutong Zhang, Bharath Hariharan, Noah Snavely, and William T. Freeman. Unsupervised semantic segmentation by distilling feature correspondences. In *International Conference on Learning Representations*, 2022.

[31] Kaiming He, Xinlei Chen, Saining Xie, Yanghao Li, Piotr Dollár, and Ross Girshick. Masked Autoencoders Are Scalable Vision Learners. *arXiv:2111.06377 [cs]*, December 2021.

[32] Kaiming He, Haoqi Fan, Yuxin Wu, Saining Xie, and Ross Girshick. Momentum Contrast for Unsupervised Visual Representation Learning. In *2020 IEEE/CVF Conference on Computer Vision and Pattern Recognition (CVPR)*, pages 9726–9735, June 2020.

[33] Kaiming He, Georgia Gkioxari, Piotr Dollár, and Ross Girshick. Mask R-CNN. In *2017 IEEE International Conference on Computer Vision (ICCV)*, pages 2980–2988, October 2017.

[34] Kaiming He, Xiangyu Zhang, Shaoqing Ren, and Jian Sun. Deep Residual Learning for Image Recognition. In *2016 IEEE Conference on Computer Vision and Pattern Recognition (CVPR)*, pages 770–778, June 2016.

[35] Olivier J. Hénaff, Skanda Koppula, Jean-Baptiste Alayrac, Aaron van den Oord, Oriol Vinyals, and João Carreira. Efficient Visual Pretraining With Contrastive Detection. In *Proceedings of the IEEE/CVF International Conference on Computer Vision*, pages 10086–10096, 2021.

[36] Olivier J. Hénaff, Skanda Koppula, Evan Shelhamer, Daniel Zoran, Andrew Jaegle, Andrew Zisserman, João Carreira, and Relja Arandjelović. Object discovery and representation networks. *arXiv:2203.08777 [cs]*, March 2022.

[37] R. Devon Hjelm, Alex Fedorov, Samuel Lavoie-Marchildon, Karan Grewal, Phil Bachman, Adam Trischler, and Yoshua Bengio. Learning deep representations by mutual information estimation and maximization. In *International Conference on Learning Representations*, September 2018.

[38] Haiyang Huang, Zhi Chen, and Cynthia Rudin. SegDiscover: Visual Concept Discovery via Unsupervised Semantic Segmentation. *arXiv:2204.10926 [cs]*, April 2022.

[39] Jyh-Jing Hwang, Stella X Yu, Jianbo Shi, Maxwell D Collins, Tien-Ju Yang, Xiao Zhang, and Liang-Chieh Chen. Segsort: Segmentation by discriminative sorting of segments. In *Proceedings of the IEEE/CVF International Conference on Computer Vision*, pages 7334–7344, 2019.

[40] Jang Hyun Cho, Utkarsh Mall, Kavita Bala, and Bharath Hariharan. PiCIE: Unsupervised Semantic Segmentation using Invariance and Equivariance in Clustering. In *2021 IEEE/CVF Conference on Computer Vision and Pattern Recognition (CVPR)*, pages 16789–16799, Nashville, TN, USA, June 2021. IEEE.

[41] Xu Ji, João F Henriques, and Andrea Vedaldi. Invariant information clustering for unsupervised image classification and segmentation. In *Proceedings of the IEEE International Conference on Computer Vision*, pages 9865–9874, 2019.

[42] Thomas Kipf, Gamaleldin F. Elsayed, Aravindh Mahendran, Austin Stone, Sara Sabour, Georg Heigold, Rico Jonschkowski, Alexey Dosovitskiy, and Klaus Greff. Conditional Object-Centric Learning from Video. *arXiv:2111.12594 [cs, stat]*, March 2022.

[43] Thomas Kipf, Elise van der Pol, and Max Welling. Contrastive Learning of Structured World Models. In *International Conference on Learning Representations*, September 2019.

[44] Philipp Krähenbühl and Vladlen Koltun. Efficient Inference in Fully Connected CRFs with Gaussian Edge Potentials. In *Advances in Neural Information Processing Systems*, volume 24. Curran Associates, Inc., 2011.

[45] H. W. Kuhn. The Hungarian method for the assignment problem. *Naval Research Logistics Quarterly*, 2(1-2):83–97, 1955.

[46] Chunyuan Li, Jianwei Yang, Pengchuan Zhang, Mei Gao, Bin Xiao, Xiyang Dai, Lu Yuan, and Jianfeng Gao. Efficient Self-supervised Vision Transformers for Representation Learning. *arXiv:2106.09785 [cs]*, June 2021.

[47] Tsung-Yi Lin, Piotr Dollár, Ross Girshick, Kaiming He, Bharath Hariharan, and Serge Belongie. Feature Pyramid Networks for Object Detection. In *2017 IEEE Conference on Computer Vision and Pattern Recognition (CVPR)*, pages 936–944, July 2017.

[48] Tsung-Yi Lin, Michael Maire, Serge Belongie, James Hays, Pietro Perona, Deva Ramanan, Piotr Dollár, and C. Lawrence Zitnick. Microsoft COCO: Common Objects in Context. In David Fleet, Tomas Pajdla, Bernt Schiele, and Tinne Tuytelaars, editors, *Computer Vision – ECCV 2014*, pages 740–755, Cham, 2014. Springer International Publishing.

[49] Songtao Liu, Zeming Li, and Jian Sun. Self-EMD: Self-Supervised Object Detection without ImageNet. *arXiv:2011.13677 [cs]*, March 2021.

[50] Francesco Locatello, Dirk Weissenborn, Thomas Unterthiner, Aravindh Mahendran, Georg Heigold, Jakob Uszkoreit, Alexey Dosovitskiy, and Thomas Kipf. Object-centric learning with slot attention. In H. Larochelle, M. Ranzato, R. Hadsell, M. F. Balcan, and H. Lin, editors, *Advances in Neural Information Processing Systems*, volume 33, pages 11525–11538. Curran Associates, Inc., 2020.

[51] Jonathan Long, Evan Shelhamer, and Trevor Darrell. Fully convolutional networks for semantic segmentation. In *2015 IEEE Conference on Computer Vision and Pattern Recognition (CVPR)*, pages 3431–3440, June 2015.

[52] Ilya Loshchilov and Frank Hutter. SGDR: Stochastic Gradient Descent with Warm Restarts. *arXiv:1608.03983 [cs, math]*, May 2017.

[53] Sindy Löwe, Klaus Greff, Rico Jonschkowski, Alexey Dosovitskiy, and Thomas Kipf. Learning Object-Centric Video Models by Contrasting Sets. *arXiv:2011.10287 [cs]*, November 2020.

[54] Mehdi Noroozi and Paolo Favaro. Unsupervised Learning of Visual Representations by Solving Jigsaw Puzzles. In Bastian Leibe, Jiri Matas, Nicu Sebe, and Max Welling, editors, *Computer Vision – ECCV 2016*, pages 69–84, Cham, 2016. Springer International Publishing.

[55] Mehdi Noroozi, Hamed Pirsiavash, and Paolo Favaro. Representation Learning by Learning to Count. In *2017 IEEE International Conference on Computer Vision (ICCV)*, pages 5899–5907, October 2017.

[56] Pedro O O. Pinheiro, Amjad Almahairi, Ryan Benmalek, Florian Golemo, and Aaron C Courville. Unsupervised learning of dense visual representations. In H. Larochelle, M. Ranzato, R. Hadsell, M. F. Balcan, and H. Lin, editors, *Advances in Neural Information Processing Systems*, volume 33, pages 4489–4500. Curran Associates, Inc., 2020.

[57] Deepak Pathak, Philipp Krähenbühl, Jeff Donahue, Trevor Darrell, and Alexei A. Efros. Context Encoders: Feature Learning by Inpainting. In *2016 IEEE Conference on Computer Vision and Pattern Recognition (CVPR)*, pages 2536–2544, June 2016.

[58] Ramprasaath R. Selvaraju, Karan Desai, Justin Johnson, and Nikhil Naik. CASTing Your Model: Learning to Localize Improves Self-Supervised Representations. In *2021 IEEE/CVF Conference on Computer Vision and Pattern Recognition (CVPR)*, pages 11053–11062, June 2021.

[59] Antti Tarvainen and Harri Valpola. Mean teachers are better role models: Weight-averaged consistency targets improve semi-supervised deep learning results. In *Advances in Neural Information Processing Systems*, volume 30. Curran Associates, Inc., 2017.

[60] Yonglong Tian, Chen Sun, Ben Poole, Dilip Krishnan, Cordelia Schmid, and Phillip Isola. What makes for good views for contrastive learning? In H. Larochelle, M. Ranzato, R. Hadsell, M. F. Balcan, and H. Lin, editors, *Advances in Neural Information Processing Systems*, volume 33, pages 6827–6839. Curran Associates, Inc., 2020.

[61] J. R. R. Uijlings, K. E. A. van de Sande, T. Gevers, and A. W. M. Smeulders. Selective Search for Object Recognition. *International Journal of Computer Vision*, 104(2):154–171, September 2013.

[62] Aaron van den Oord, Yazhe Li, and Oriol Vinyals. Representation Learning with Contrastive Predictive Coding. *arXiv:1807.03748 [cs, stat]*, January 2019.

[63] Wouter Van Gansbeke, Simon Vandenhende, Stamatios Georgoulis, and Luc V Gool. Revisiting contrastive methods for unsupervised learning of visual representations. In M. Ranzato, A. Beygelzimer, Y. Dauphin, P.S. Liang, and J. Wortman Vaughan, editors, *Advances in Neural Information Processing Systems*, volume 34, pages 16238–16250. Curran Associates, Inc., 2021.

[64] Wouter Van Gansbeke, Simon Vandenhende, Stamatios Georgoulis, and Luc Van Gool. Unsupervised Semantic Segmentation by Contrasting Object Mask Proposals. In *Proceedings of the IEEE/CVF International Conference on Computer Vision*, pages 10052–10062, 2021.

[65] Ashish Vaswani, Noam Shazeer, Niki Parmar, Jakob Uszkoreit, Llion Jones, Aidan N. Gomez, Łukasz Kaiser, and Illia Polosukhin. Attention is all you need. In *Proceedings of the 31st International Conference on Neural Information Processing Systems*, NIPS'17, pages 6000–6010, Red Hook, NY, USA, December 2017. Curran Associates Inc.

[66] Pascal Vincent, Hugo Larochelle, Yoshua Bengio, and Pierre-Antoine Manzagol. Extracting and composing robust features with denoising autoencoders. In *Proceedings of the 25th International Conference on Machine Learning - ICML '08*, pages 1096–1103, Helsinki, Finland, 2008. ACM Press.

[67] Xinlong Wang, Zhiding Yu, Shalini De Mello, Jan Kautz, Anima Anandkumar, Chunhua Shen, and Jose M Alvarez. Freesolo: Learning to segment objects without annotations. In *Proceedings of the IEEE/CVF Conference on Computer Vision and Pattern Recognition*, pages 14176–14186, 2022.

[68] Xinlong Wang, Rufeng Zhang, Chunhua Shen, Tao Kong, and Lei Li. Dense Contrastive Learning for Self-Supervised Visual Pre-Training. In *2021 IEEE/CVF Conference on Computer Vision and Pattern Recognition (CVPR)*, pages 3023–3032, Nashville, TN, USA, June 2021. IEEE.

[69] Chen Wei, Haoqi Fan, Saining Xie, Chao-Yuan Wu, Alan Yuille, and Christoph Feichtenhofer. Masked Feature Prediction for Self-Supervised Visual Pre-Training. *arXiv:2112.09133 [cs]*, December 2021.

[70] Fangyun Wei, Yue Gao, Zhirong Wu, Han Hu, and Stephen Lin. Aligning Pretraining for Detection via Object-Level Contrastive Learning. In *Advances in Neural Information Processing Systems*, volume 34, pages 22682–22694. Curran Associates, Inc., 2021.

[71] Yuxin Wu, Alexander Kirillov, Francisco Massa, Wan-Yen Lo, and Ross Girshick. Detectron2. `https://github.com/facebookresearch/detectron2`, 2019.

[72] Zhirong Wu, Yuanjun Xiong, Stella X. Yu, and Dahua Lin. Unsupervised Feature Learning via Non-parametric Instance Discrimination. In *2018 IEEE/CVF Conference on Computer Vision and Pattern Recognition*, pages 3733–3742, June 2018.

[73] Enze Xie, Jian Ding, Wenhai Wang, Xiaohang Zhan, Hang Xu, Peize Sun, Zhenguo Li, and Ping Luo. DetCo: Unsupervised Contrastive Learning for Object Detection. In *Proceedings of the IEEE/CVF International Conference on Computer Vision*, pages 8392–8401, 2021.

[74] Jiahao Xie, Xiaohang Zhan, Ziwei Liu, Yew Soon Ong, and Chen Change Loy. Unsupervised object-level representation learning from scene images. In M. Ranzato, A. Beygelzimer, Y. Dauphin, P.S. Liang, and J. Wortman Vaughan, editors, *Advances in Neural Information Processing Systems*, volume 34, pages 28864–28876. Curran Associates, Inc., 2021.

[75] Zhenda Xie, Yutong Lin, Zheng Zhang, Yue Cao, Stephen Lin, and Han Hu. Propagate Yourself: Exploring Pixel-Level Consistency for Unsupervised Visual Representation Learning. In *2021 IEEE/CVF Conference on Computer Vision and Pattern Recognition (CVPR)*, pages 16679–16688, Nashville, TN, USA, June 2021. IEEE.

[76] Ceyuan Yang, Zhirong Wu, Bolei Zhou, and Stephen Lin. Instance Localization for Self-supervised Detection Pretraining. In *2021 IEEE/CVF Conference on Computer Vision and Pattern Recognition (CVPR)*, pages 3986–3995, June 2021.

[77] Charig Yang, Hala Lamdouar, Erika Lu, Andrew Zisserman, and Weidi Xie. Self-Supervised Video Object Segmentation by Motion Grouping. In *Proceedings of the IEEE/CVF International Conference on Computer Vision*, pages 7177–7188, 2021.

[78] Asano Ym, Rupprecht C, and Vedaldi A. Self-labelling via simultaneous clustering and representation learning. In *International Conference on Learning Representations*, September 2019.

[79] Yang You, Igor Gitman, and Boris Ginsburg. Large Batch Training of Convolutional Networks. *arXiv:1708.03888 [cs]*, September 2017.

[80] Fisher Yu, Haofeng Chen, Xin Wang, Wenqi Xian, Yingying Chen, Fangchen Liu, Vashisht Madhavan, and Trevor Darrell. Bdd100k: A diverse driving dataset for heterogeneous multitask learning. In *Proceedings of the IEEE/CVF conference on computer vision and pattern recognition*, pages 2636–2645, 2020.

[81] Jure Zbontar, Li Jing, Ishan Misra, Yann LeCun, and Stephane Deny. Barlow Twins: Self-Supervised Learning via Redundancy Reduction. In *Proceedings of the 38th International Conference on Machine Learning*, pages 12310–12320. PMLR, July 2021.

[82] Richard Zhang, Phillip Isola, and Alexei A. Efros. Colorful Image Colorization. In Bastian Leibe, Jiri Matas, Nicu Sebe, and Max Welling, editors, *Computer Vision – ECCV 2016*, pages 649–666, Cham, 2016. Springer International Publishing.

[83] Richard Zhang, Phillip Isola, and Alexei A. Efros. Split-Brain Autoencoders: Unsupervised Learning by Cross-Channel Prediction. In *2017 IEEE Conference on Computer Vision and Pattern Recognition (CVPR)*, pages 645–654, July 2017.

[84] Xiao Zhang and Michael Maire. Self-supervised visual representation learning from hierarchical grouping. In H. Larochelle, M. Ranzato, R. Hadsell, M. F. Balcan, and H. Lin, editors, *Advances in Neural Information Processing Systems*, volume 33, pages 16579–16590. Curran Associates, Inc., 2020.

[85] Bingchen Zhao and Xin Wen. Distilling Visual Priors from Self-Supervised Learning. In Adrien Bartoli and Andrea Fusiello, editors, *Computer Vision – ECCV 2020 Workshops*, pages 422–429, Cham, 2020. Springer International Publishing.

[86] Bolei Zhou, Hang Zhao, Xavier Puig, Tete Xiao, Sanja Fidler, Adela Barriuso, and Antonio Torralba. Semantic Understanding of Scenes Through the ADE20K Dataset. *International Journal of Computer Vision*, 127(3):302–321, March 2019.

[87] Rui Zhu, Bingchen Zhao, Jingen Liu, Zhenglong Sun, and Chang Wen Chen. Improving Contrastive Learning by Visualizing Feature Transformation. *arXiv:2108.02982 [cs]*, August 2021.

[88] Adrian Ziegler and Yuki M. Asano. Self-Supervised Learning of Object Parts for Semantic Segmentation. *arXiv:2204.13101 [cs]*, April 2022.

Checklist

1. For all authors...
   (a) Do the main claims made in the abstract and introduction accurately reflect the paper's contributions and scope? [Yes]
   (b) Did you describe the limitations of your work? [Yes] The limitations are discussed in Section G.
   (c) Did you discuss any potential negative societal impacts of your work? [Yes] The potential negative societal impacts are discussed in Section G.
   (d) Have you read the ethics review guidelines and ensured that your paper conforms to them? [Yes]
2. If you are including theoretical results...
   (a) Did you state the full set of assumptions of all theoretical results? [N/A]
   (b) Did you include complete proofs of all theoretical results? [N/A]
3. If you ran experiments...
   (a) Did you include the code, data, and instructions needed to reproduce the main experimental results (either in the supplemental material or as a URL)? [Yes] Link to the code is provided in the abstract.
   (b) Did you specify all the training details (e.g., data splits, hyperparameters, how they were chosen)? [Yes]
   (c) Did you report error bars (e.g., with respect to the random seed after running experiments multiple times)? [N/A]
   (d) Did you include the total amount of compute and the type of resources used (e.g., type of GPUs, internal cluster, or cloud provider)? [Yes]
4. If you are using existing assets (e.g., code, data, models) or curating/releasing new assets...
   (a) If your work uses existing assets, did you cite the creators? [Yes]
   (b) Did you mention the license of the assets? [Yes]
   (c) Did you include any new assets either in the supplemental material or as a URL? [N/A]
   (d) Did you discuss whether and how consent was obtained from people whose data you're using/curating? [N/A]
   (e) Did you discuss whether the data you are using/curating contains personally identifiable information or offensive content? [N/A]
5. If you used crowdsourcing or conducted research with human subjects...
   (a) Did you include the full text of instructions given to participants and screenshots, if applicable? [N/A]
   (b) Did you describe any potential participant risks, with links to Institutional Review Board (IRB) approvals, if applicable? [N/A]
   (c) Did you include the estimated hourly wage paid to participants and the total amount spent on participant compensation? [N/A]

Appendix

A Additional implementation details

A.1 Inverse augmentation

The inverse augmentation process aims to recover the original pixel locations and ensure the two feature maps produced from two augmented views are spatially aligned after inverse augmentation. There are two operations in our data augmentation pipeline that changes the scale or layout of the image, *i.e.*, random resized crop and random horizontal flip. Since we already know the spatial coordinates where each view is cropped from, we can map the coordinates to the corresponding feature maps and cut the rectangular part from the feature map where the two sets of coordinates intersect. This is followed by a resize operation to recover the intersect part to the original size (*e.g.*, 7×7 for a 224×224 input). In implementation, we achieve this through RoIAlign [33]. If the horizontal flip operation is applied to produce the view, we also use a horizontal flip operation after RoIAlign to recover the original spatial layout. After the inverse augmentation, each pixel in the two feature maps is spatial-aligned, making applying the per-pixel cross-entropy loss easy.

A.2 Transfer learning

A.2.1 Object detection and instance segmentation

We train a Mask R-CNN [33] model with R50-FPN backbone [47] implemented with the open-source project `Detectron2` [71], following the same fine-tuning setup with [68, 75, 74]. Specifically, we use a batch size of 16, and fine-tune for 90k iterations (standard $1\times$ schedule) with batch normalization layers synchronized. The learning rate is initialized as 0.02 with a linear warm-up for 1000 iterations, and decayed by 0.1 at 60k and 80k iterations. The image scale is $[640, 800]$ during training and 800 at inference. We fine-tune all layers end-to-end on COCO [48] `train2017` set with the standard $1\times$ schedule and report AP, AP_{50}, AP_{75} on the `val2017` set.

A.2.2 Semantic segmentation

Cityscapes and PASCAL VOC. We strictly follow [32] for transfer learning on these two datasets. Specifically, we use the same fully-convolutional network (FCN)-based [51] architecture as [32]. The backbone consists of the convolutional layers in ResNet-50, in which the 3×3 convolutions in conv5 blocks have dilation 2 and stride 1. This is followed by two extra 3×3 convolutions of 256 channels (dilation set to 6), with batch normalization and ReLU activations, and then a 1×1 convolution for per-pixel classification. The total stride is 16 (FCN-16s [51]).

Training is performed with random scaling (by a ratio in $[0.5, 2.0]$), cropping, and horizontal flipping. The crop size is 513 on PASCAL VOC [20] and 769 on Cityscapes [13], and inference is performed on the original image size. We train with batch size 16 and weight decay 0.0001. The learning rate is 0.003 on VOC and is 0.01 on Cityscapes (multiplied by 0.1 at the 70th and 90th percentile of training). For PASCAL VOC, we fine-tune the model on `train_aug2012` set for 30k iterations and report the mean intersection over union (mIoU) on the `val2012` set. For Cityscapes, we fine-tune on the `train_fine` set for 90k iterations and evaluate it on the `val_fine` set.

ADE20K. For ADE20K [86], we train with a FCN-8s [51] model on the `train` set and evaluate on the `val` set, and the optimization specifics follows the standard 80k iterations schedule of `MMSegmentation` [12]. Specifically, we fine-tune for 80k iterations with stochastic gradient descent, with a batch size of 16 and weight decay of 0.0005. The learning rate is 0.01 and decays following the poly schedule with power of 0.9 and min_lr of 0.0001.

A.3 Unsupervised semantic segmentation

Experiment setting. We follow the common practice in this field [41, 40, 38] to use a modified version of COCO-Stuff [4], where the labels are merged into 27 categories (15 "stuff" categories and 12 "thing" categories). We perform inference with resolution 320 and number of prototypes 27 following the common practice, and evaluate on mIoU and pixel accuracy (pAcc).

Inference details. Intuitively, each prototype can be viewed as the cluster center of a semantic class. Therefore, we simply adopt the prototypes $\mathcal{S} \in \mathbb{R}^{K \times D}$ as a 1×1 convolution layer for per-pixel classification, and predict the prototypical correspondence of each pixel with the argmax operation.

$$\hat{y} = \operatorname*{argmax}_{K} \left(\operatorname{resize} \left(\overline{\boldsymbol{z}} \cdot \overline{\mathcal{S}}^{\top} \right) \right) \in \mathbb{Z}^{H' \times W'} , \tag{9}$$

where the resize operation denotes bi-linear interpolation on the logits to the size of the image (320×320 in this case). To match the prototypes with the ground truth clusters, we follow the standard protocol [41, 40] of finding the best one-to-one permutation mapping using Hungarian-matching [45]. Then the pAcc and mIoU are calculated according to the common practice [40]. During inference, we only take the teacher model parameterized by ξ.

A.4 Visual concept discovery

Simply speaking, the visual concept discovery is similar to the semantic segment retrieval task [63], except that the queries are prototypes rather than segments. Specifically, we adopt the COCO `val2017` set, consisting of 5k images, and the default model trained on COCO with the number of prototypes $K = 256$. Each image is first resized to 256 pixels along the shorter side, after which a 224×224 center crop is applied. We then follow Eq. 9 to assign a prototype index to each pixel; thus, each image is split into a set of groups, such that the pixels within each group hold the same prototypical assignments. We rephrase the groups as *segments*, and compute the feature vector for each segment by average pooling. Then for each prototype, we calculate the cosine similarity between it and all segments in the dataset assigned to this prototype and retrieve those with top-k high similarity scores.

A.5 Re-implementing related works

Some current works may differ in implementation details for downstream tasks (*e.g.*, SoCo [70] uses different hyper-parameters for COCO object detection and instance segmentation, DetCon [35] uses different hyper-parameters for semantic segmentation, and DenseCL [68] adopts different network architectures for semantic segmentation). For a fair comparison, we re-produced the transfer learning results with a unified setting with the official checkpoints and re-implement the pre-training with the official code if needed.

B Additional transfer learning results

B.1 Longer COCO schedule

Table 6: **Additional transfer learning results with COCO 800 epochs pre-training.** We report the results in COCO object detection and COCO instance segmentation with both $1\times$ and $2\times$ schedules.

Method	Transfer learning schedule	COCO detection			COCO segmentation		
		AP^b	AP^b_{50}	AP^b_{75}	AP^m	AP^m_{50}	AP^m_{75}
SlotCon	$1\times$ (90k iterations)	41.0	61.1	45.0	37.0	58.3	39.8
SlotCon	$2\times$ (180k iterations)	42.6	62.7	46.2	38.2	59.6	41.0

In Table 6, we further provide the downstream results of SlotCon in COCO object detection and instance segmentation with a longer transfer learning schedule ($2\times$). Compared with the results with the $1\times$ schedule, it shows significant improvements in all metrics.

B.2 Pre-training with autonomous driving data

In Table 7, we show the results with BDD100K [80] pre-training and evaluated on Cityscapes semantic segmentation. The model is trained on BDD100K for 800 epochs with 64 prototypes. The result is notably weaker than its COCO counterpart, yet still surpasses MoCo v2 pre-trained on COCO. The BDD100K dataset is indeed challenging for pre-training as its images are less discriminative, and the task of pre-training on autonomous driving data is a valuable direction for future explorations.

Table 7: Transfer learning results with BDD100K pre-training.

Pre-train Data	Method	Cityscapes mIoU
-	Random init.	65.3
COCO	MoCo v2	73.8
COCO	SlotCon	76.2
BDD100K	SlotCon	73.9

C Additional ablation studies

Table 8: **Ablation studies with COCO 800 epochs pre-training.** We show the AP^b on COCO objection detection and mIoU on Cityscapes, PASCAL VOC, and ADE20K semantic segmentation. The default options are marked with a gray background.

(a) **Batch size**

B	COCO	City	VOC	ADE
256	40.6	75.9	70.9	38.1
512	**41.0**	**76.2**	71.6	**39.0**
1024	40.7	75.7	**71.8**	38.6

(b) **Type of group-level loss**

Loss	COCO	City	VOC	ADE
Reg.	40.7	75.9	71.0	**39.0**
Ctr.	**41.0**	**76.2**	**71.6**	**39.0**

(c) **Where to apply** invaug**?**

Align	COCO	City	VOC	ADE
Proj.	40.9	75.7	71.4	38.0
Asgn.	**41.0**	**76.2**	**71.6**	**39.0**

(d) **Batch size and image-level objective**

B	$\mathcal{L}_{\text{Image}}$	COCO AP^b	COCO AP^m
512	✗	41.0	**37.0**
512	✓	40.8	36.8
1024	✗	40.7	36.7
1024	✓	**41.1**	**37.0**

(e) **Geometric augmentations**

Method	Geometric aug.	VOC mIoU
Random init.	-	39.5
SlotCon	✓	**71.6**
SlotCon	✗	62.6

In Table 8, we provide the results of further ablation studies in batch size, the type of group-level contrastive loss, the place to apply inverse augmentation, the influence of an image-level learning objective, and the importance of geometric augmentations. We discuss them as follows:

Batch size. Table 8a shows the most suitable batch size for our method is 512. Increasing it to 1024 does not result in better performance. We argue that the real slot-level batch size is actually bigger than 512, and should be multiplied by the number of pixels (49) or slots (~ 8) per image for the grouping loss and the group-level contrastive loss, respectively. Considering the mismatch in the batch size scale of the two loss functions, the learning rate might should be further tuned to work with larger batches [26].

Type of group-level loss. Table 8b shows that both the BYOL [29]-style regression loss and the contrastive loss are helpful to learning transferable features, and the results with the contrastive loss are especially higher for object detection in COCO. This may indicate that the contrastive loss, which better pushes negative samples apart, is beneficial for object detection, in which the ability to tell confusing objects apart is also critical.

Place to apply inverse augmentation. Table 8c ablates whether to apply the inverse augmentation operation on the dense projections or the grouping assignments, and shows the latter is better. This can keep the non-overlapping features for the group-level contrastive loss and utilize more information.

Image-level learning objective. Table 8d ablates the effect of an auxiliary image-level learning objective. We add a MoCo v3 [11] style image-level contrastive learning loss to SlotCon (COCO 800 epoch pre-training setting), and the experiment results on COCO show that it depends on the batch size. With a smaller batch size of 512, the detection AP drops by 0.2 points, while with a higher batch size of 1024, the detection AP rises by 0.4 points. Our explanation is that the image-level objective is more sensitive to the batch size, and it requires a larger batch size to learn holistic representations that are complementary to the object-level objective.

Geometric augmentations. Table 8e ablates the effect of the geometric augmentations. Our main finding is that geometric augmentations are necessary to learn object-centric representations in our setting. We train SlotCon on COCO for 800 epochs with two identical crops applied for each image, thus only the photometric invariance is adopted as the supervision. We then visualized the slots the same way as Figure 3, and found that almost none of the slots can bind to a meaningful semantic. Most of them attend to a similar-shaped region that locates at the same position across different images while holding diverging semantics. And some of them learn textures like animal fur, cloudy sky, snowland, or leaves. A fast evaluation on PASCAL VOC semantic segmentation shows a significant performance drop, yet the feature is still notably better than random initialization.

D Statistics about the binary indicator

How many slots are active on average for each image? It depends on the number of categories/semantics per image. As in Figure 4 of the supplementary file, 7 slots are active on average for one image after convergence.

How often is one slot active over the whole dataset? It depends on the category/semantic distribution of the dataset, as the slots are roughly bound to real-world semantic categories. We studied the activeness of the slots over the COCO `val2017` set that contains 5000 images, and found that 40 out of the 256 slots are dead, and not active to any image. The activeness of the remaining slots follows a long-tailed distribution. The top-5 active slots correspond to tree (376), sky (337), streetside car (327), building exterior wall (313), and indoor wall (307); and the bottom-5 active slots correspond to skateboarder (44), grassland (45), train (56), luggage (57), and airplane (57).

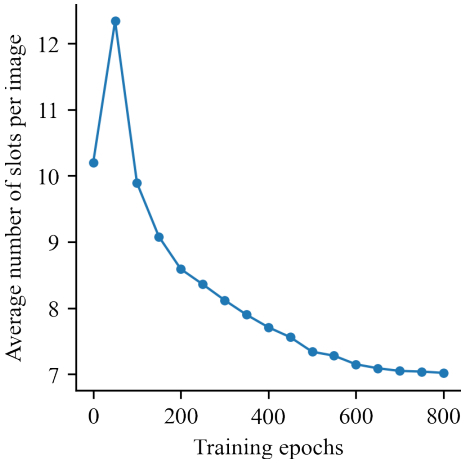

Figure 4: Average number of active slots per image during training on COCO.

How many terms are excluded in Eq. 6? Given the slot number as 256, if all slots are active for one image and the two crops overlap well, there should be 256 positive pairs. We studied a well-converged model and found that, on average, only around 3.6 pairs are active, so around 252.4 terms are excluded. It is reasonable considering that around 7 slots are active on one image, and the overlapping area between the two crops can be small. Considering a total batch size of 512, the number of excluded negative samples should be around $512 \times (256 - 7) = 127488$.

E Computational costs

In Table 8 we give a direct computational cost comparison between SlotCon and two previous works. The experiments are conducted on the same machine with 8 NVIDIA GeForce RTX 3090 GPUs. Both PixPro and SlotCon adopt a batch size of 1024 and have amp turned on, and DenseCL adopts a batch size of 256 by default. The training time of DenseCL might be higher than optimal as we failed to install apex.

Table 8: Computational cost evaluation.

Method	Time/epoch	Memory/GPU
DenseCL [68]	$2'46''$	7.9 GB
PixPro [75]	$2'19''$	15.1 GB
SlotCon	$2'23''$	16.0 GB

F Additional qualitative results

Unsupervised semantic segmentation. In Figure 5, 6, 7, we provide the visualization of more results in COCO-Stuff unsupervised semantic segmentation. Compared with PiCIE [40], our method's overall successes in distinguishing confusing objects apart and localizing small objects.

Visual concept discovery on COCO. In Figure 8, 9, we show more results of visual concepts discovered by our model from COCO, which cover a wide range of natural scenes. We further show that the model tends to categorize person-related concepts into fine-grained clusters. For example, in Figure 10, we show that it also groups segments according to the part of the human body; and in Figure 11, we show that it also groups person segments by the sport they are playing. We hypothesize that persons are too common in COCO, and the model finds that allocating more prototypes to learn person-related concepts can better help optimize the grouping loss.

Visual concept discovery on ImageNet. In Figure 12, 13 we also provide examples of visual concepts discovered by our method from ImageNet. Due to the scale of ImageNet, it is hard to compute the segments for all the images. As ImageNet is basically single-object-centric, we simply treat each image as a single segment to save computation for nearest-neighbor searching. The visualization verifies the compatibility of our method with object-centric data.

G Limitations and negative social impacts

Grouping precision. Since we directly learn a set of semantic prototypes with a quite low-resolution feature map ($32\times$ downsample) and do not have any supervision for precise object boundaries, it is hard for our model to perform detailed semantic grouping and cases are that many foreground instances are segmented with over-confidence. Using post-processing through iterative refinements such as CRF [44] or pre-compute visual primitives (super-pixels) on the raw image [38] may improve the result, but they are out of the scope of this work. Besides, modern object discovery techniques such as Slot Attention [50] that incorporate attention mechanism and iterative refinement may also help learn better semantic groups; we leave this for future work.

Training cost. As all self-supervised learning methods do, our approach also needs to pre-train with multiple GPU devices for a long time, which may increase carbon emissions. However, for one thing, the pre-training only needs to be done once and can help reduce the training time of multiple downstream tasks; for another, our method can learn relatively good representations with shorter training time, *e.g.*, our method pre-trained on ImageNet for 100 epochs achieves compatible performance with PixPro [75] pre-trained for 400 epochs in COCO objection detection ($\text{AP}^{\text{b}} = 41.4$).

The data can be unreliable. With reduced human priors, our method learns to discover objects/semantics form large-scale natural images. However, totally relying on the data may lead to "bad" biases. In our experiments on scene-centric data, we noticed that the model allocates more prototypes to human-related concepts (as humans occur most frequently in COCO), while many other kinds of animals only have one prototype (see Figure 9, 11, 10). When pre-training on a more long-tailed and less discriminative scenario (*e.g.*, autonomous driving data, detailed in Sec B.2), the data can lead to highly biased prototypes and representations, and harm downstream performance. Injecting human priors to guide the criterion for objects/semantics could be a promising direction.

Semantic rather than object. Our method performs semantic grouping; this means that objects with identical semantics can be indistinguishable. Therefore, the contrastive learning objective (Eq. 7) does not contrast between objects in the same image with the same semantic (*e.g.*, two elephants in one image). However, the success of self-supervised learning has shown that discriminating instances with identical category labels can further boost representation quality. The transition from semantic to objectness is to be explored.

H License of used datasets

All the datasets used in this paper are permitted for research use. The terms of access to the images of COCO [48] and ImageNet [15] allow the use for non-commercial research and educational purposes. Besides, the annotations of COCO [48] and COCO-Stuff [4] follow the Creative Commons Attribution 4.0 License, also allowing for research purposes.

Figure 5: Additional results in COCO-Stuff [4] unsupervised semantic segmentation. Each row from top to down: Image, PiCIE [40], Ours. Overall, our method successfully distinguishes confusing objects and localizes small objects. (*best viewed in color*)

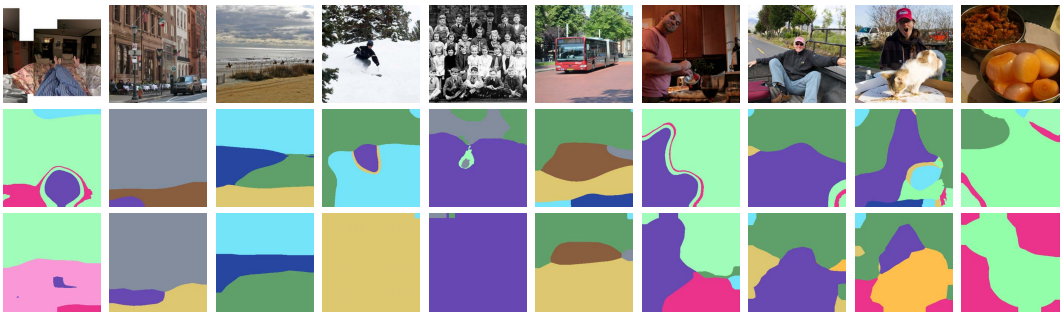

Figure 6: Additional results in COCO-Stuff [4] unsupervised semantic segmentation. Each row from top to down: Image, PiCIE [40], Ours. Overall, our method successfully distinguishes confusing objects and localizes small objects. (*best viewed in color*)

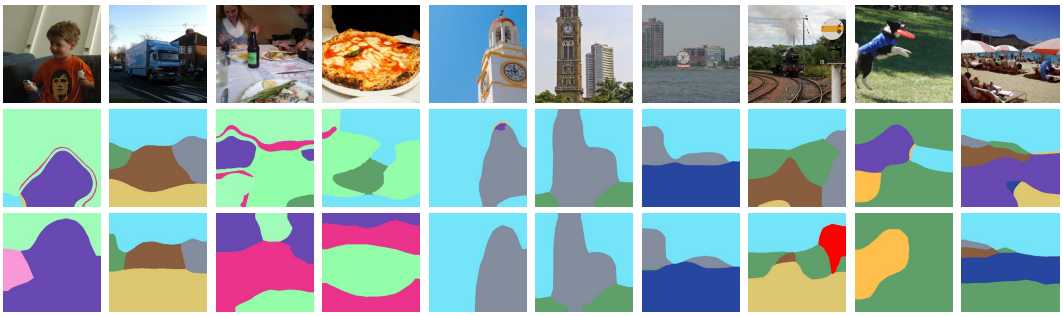

Figure 7: Additional results in COCO-Stuff [4] unsupervised semantic segmentation. Each row from top to down: Image, PiCIE [40], Ours. Overall, our method successfully distinguishes confusing objects and localizes small objects. (*best viewed in color*)

Figure 8: Additional examples of visual concepts discovered by our method from the COCO `val2017` split. Each row shows the top 10 segments retrieved with the same prototype, marked with red masks. (*best viewed in color*)

Figure 9: Additional examples of visual concepts discovered by our method from the COCO `val2017` split. Each row shows the top 10 segments retrieved with the same prototype, marked with red masks. (*best viewed in color*)

Figure 10: Additional examples of visual concepts discovered by our method from the COCO `val2017` split. Each column shows the top 5 segments retrieved with the same prototype, marked with red masks. The model tends to group person-related segments into fine-grained clusters. This figure shows those related to different granularities of the human body, including the forehead, face, shoulder & neck, hand, arm, elbow, chest, leg, and crowd. (*best viewed in color*)

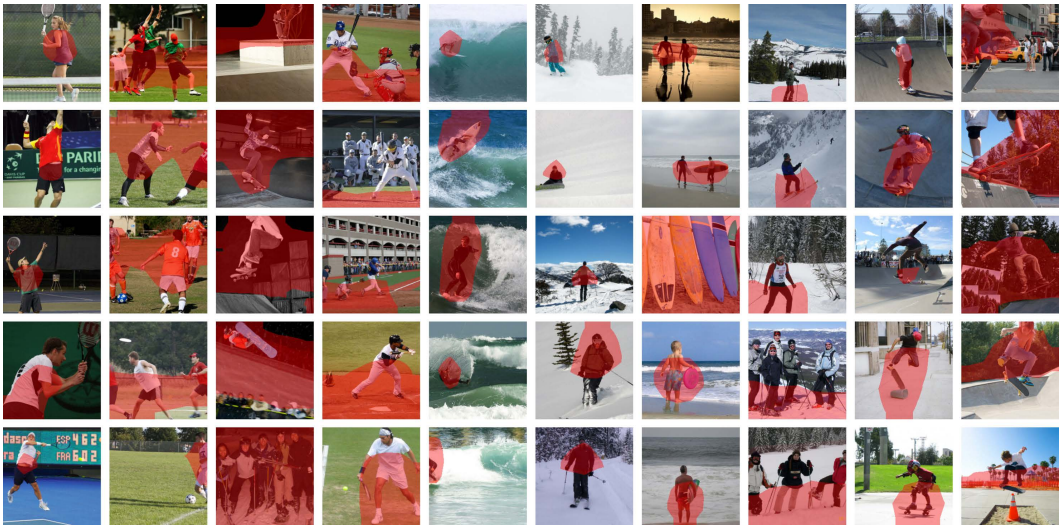

Figure 11: Additional examples of visual concepts discovered by our method from the COCO `val2017` split. Each column shows the top 5 segments retrieved with the same prototype, marked with red masks. The model tends to group person-related segments into fine-grained clusters. This figure shows those related to different types of sports, including tennis, football, skateboarding, baseball, surfing, and skiing. (*best viewed in color*)

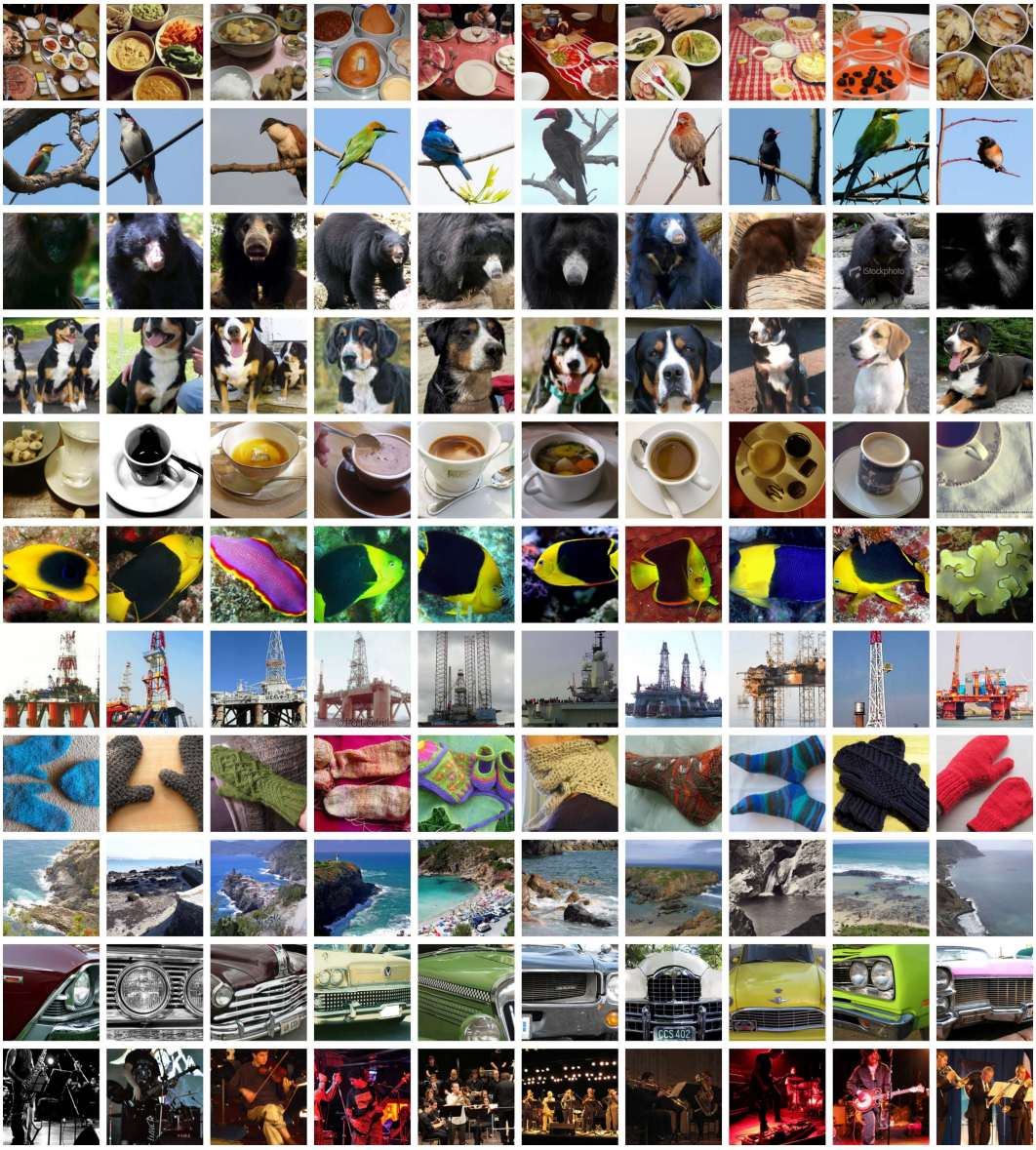

Figure 12: Additional examples of visual concepts discovered by our method from ImageNet [15]. Each row shows the top 10 images retrieved with the same prototype. Due to the scale of ImageNet, it is hard to compute the segments for all the images. As ImageNet is basically single-object-centric, we simply treat each image as a single segment to save computation for nearest-neighbor searching. The result verifies our method's compatibility with object-centric data. (*best viewed in color*)

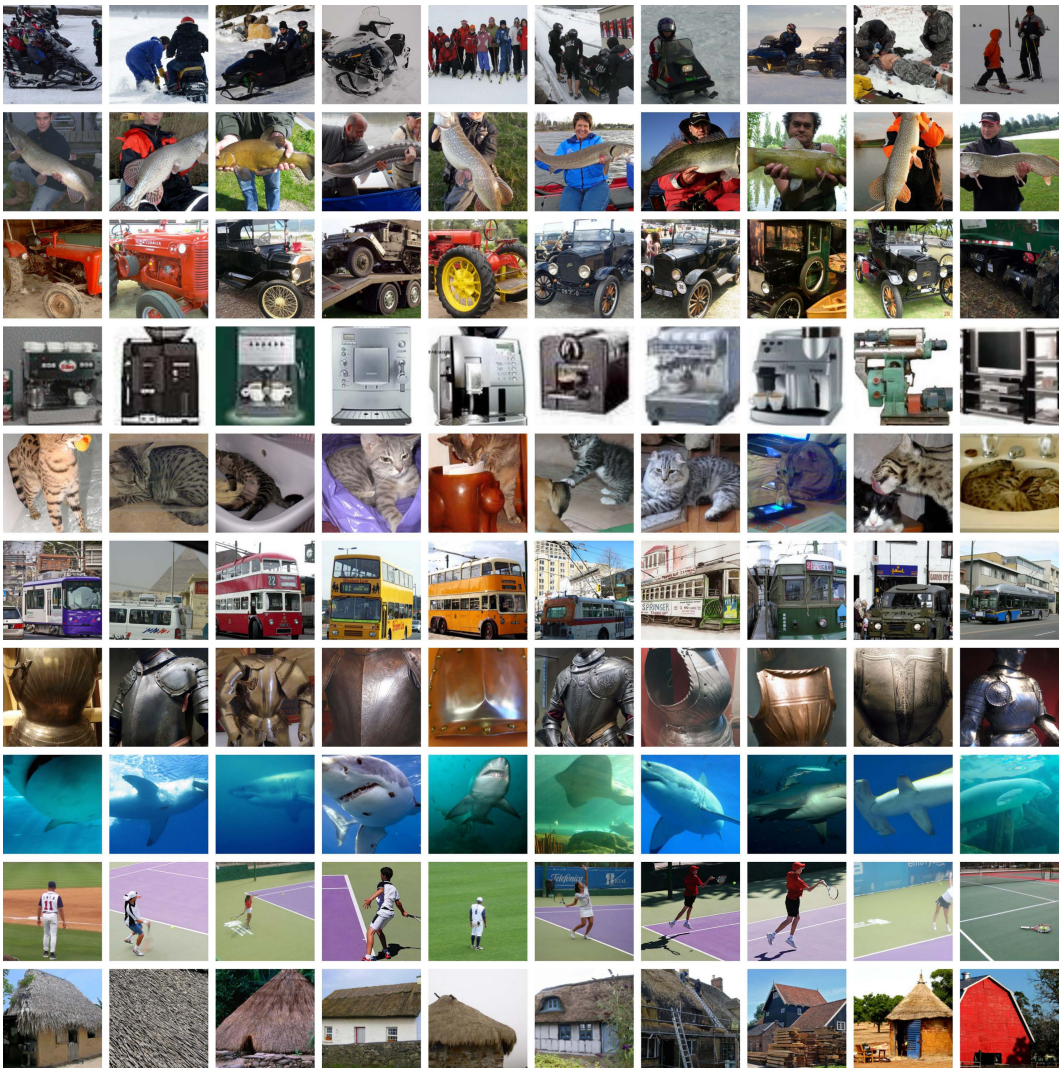

Figure 13: Additional examples of visual concepts discovered by our method from ImageNet [15]. Each row shows the top 10 images retrieved with the same prototype. Due to the scale of ImageNet, it is hard to compute the segments for all the images. As ImageNet is basically single-object-centric, we simply treat each image as a single segment to save computation for nearest-neighbor searching. The result verifies our method's compatibility with object-centric data. (*best viewed in color*)